Detecting Neuroendocrine Prostate Cancer Through Tissue-Informed Cell-Free DNA Methylation Analysis

Jacob E. Berchuck[1,2], Sylvan C. Baca[1,2], Heather M. McClure[1,2], Keegan Korthauer[3,4], Harrison K. Tsai[5], Pier Vitale Nuzzo[1,2], Kaitlin M. Kelleher[1], Monica He[1], John A. Steinharter[1], Soumya Zacharia[1,2], Sandor Spisak[1,2], Ji-Heui Seo[1,2], Vincenza Conteduca[6], Olivier Elemento[7], Joonghoon Auh[7], Michael Sigouros[7], Eva Corey[8], Michelle S. Hirsch[5], Mary-Ellen Taplin[1], Toni K. Choueiri[1], Mark M. Pomerantz[1,2], Himisha Beltran[1], and Matthew L. Freedman[1,2]

ABSTRACT

Purpose: Neuroendocrine prostate cancer (NEPC) is a resistance phenotype that emerges in men with metastatic castration-resistant prostate adenocarcinoma (CR-PRAD) and has important clinical implications, but is challenging to detect in practice. Herein, we report a novel tissue–informed epigenetic approach to noninvasively detect NEPC.

Experimental Design: We first performed methylated immunoprecipitation and high-throughput sequencing (MeDIP-seq) on a training set of tumors, identified differentially methylated regions between NEPC and CR-PRAD, and built a model to predict the presence of NEPC (termed NEPC Risk Score). We then performed MeDIP-seq on cell-free DNA (cfDNA) from two independent cohorts of men with NEPC or CR-PRAD and assessed the accuracy of the model to predict the presence NEPC.

Results: The test cohort comprised cfDNA samples from 48 men, 9 with NEPC and 39 with CR-PRAD. NEPC Risk Scores were significantly higher in men with NEPC than CR-PRAD ($P = 4.3 \times 10^{-7}$) and discriminated between NEPC and CR-PRAD with high accuracy (AUROC 0.96). The optimal NEPC Risk Score cutoff demonstrated 100% sensitivity and 90% specificity for detecting NEPC. The independent, multi-institutional validation cohort included cfDNA from 53 men, including 12 with NEPC and 41 with CR-PRAD. NEPC Risk Scores were significantly higher in men with NEPC than CR-PRAD ($P = 7.5 \times 10^{-12}$) and perfectly discriminated NEPC from CR-PRAD (AUROC 1.0). Applying the predefined NEPC Risk Score cutoff to the validation cohort resulted in 100% sensitivity and 95% specificity for detecting NEPC.

Conclusions: Tissue-informed cfDNA methylation analysis is a promising approach for noninvasive detection of NEPC in men with advanced prostate cancer.

Introduction

Neuroendocrine prostate cancer (NEPC) can arise as a resistance mechanism to androgen deprivation therapy (ADT) and androgen receptor signaling inhibitors (ARSI) in men with metastatic castration-resistant prostate cancer (mCRPC; refs. 1, 2). Present in up to 17% of men with mCRPC, NEPC is associated with poor response to ARSIs and shorter overall survival (OS; refs. 1, 2). However, NEPC tumors are more likely to respond to platinum-based chemotherapy, and several novel NEPC-directed therapies are in clinical development (3).

The current approach to diagnosing NEPC—performing tissue biopsy for pathologic tumor analysis—has significant shortcomings. There is a lack of consensus pathologic criteria for defining NEPC, and due to intrapatient tumor heterogeneity, biopsy samples may not represent a patient's overall disease burden (4–6). Consequently, NEPC diagnosis is often delayed or missed, and reported rates likely underestimate the prevalence of this aggressive disease variant. The lack of a biomarker for early and accurate detection is a significant barrier to improving outcomes for men who develop NEPC.

Liquid biopsies are well-suited to address this unmet need. Most clinical cell-free DNA (cfDNA) tests detect somatically acquired tumor mutations or copy-number alterations. However, the defining genetic hallmark of NEPC, deleterious alterations in *RB1* and/or *TP53*, is present in more than one third of castration-resistant prostate adenocarcinoma (CR-PRAD) tumors and thus cannot unambiguously discriminate between the tumor subtypes (1). In contrast, vast DNA methylation differences exist between NEPC and CR-PRAD (4). Cell-free methylated DNA immunoprecipitation and high-throughput sequencing (cfMeDIP-seq), a highly sensitive method for genome-wide cfDNA methylation profiling, capable of noninvasive cancer detection and discriminating between tumor types, is well-suited to noninvasively detect NEPC (7–9).

In this article, we evaluate the ability of cfMeDIP-seq to detect NEPC in men with mCRPC. We first perform methylation profiling on a training set of NEPC and PRAD tumors to identify methylation sites enriched in each tumor type. We then establish the ability to implement tissue-informed analysis of cfMeDIP-seq data to detect NEPC in

[1]Department of Medical Oncology, Dana-Farber Cancer Institute, Harvard Medical School, Boston, Massachusetts. [2]Center for Functional Cancer Epigenetics, Dana-Farber Cancer Institute, Boston, Massachusetts. [3]Department of Statistics, University of British Columbia, Vancouver, British Columbia, Canada. [4]BC Children's Hospital Research Institute, Vancouver, British Columbia, Canada. [5]Department of Pathology, Brigham and Women's Hospital and Harvard Medical School, Boston, Massachusetts. [6]Unit of Medical Oncology and Biomolecular Therapy, Department of Medical and Surgical Sciences, University of Foggia, Foggia, Italy. [7]Englander Institute for Precision Medicine, Weill Cornell Medicine, New York, New York. [8]Department of Urology, University of Washington, Seattle, Washington.

Note: Supplementary data for this article are available at Clinical Cancer Research Online (http://clincancerres.aacrjournals.org/).

J.E. Berchuck, S.C. Baca, and H.M. McClure contributed equally to this article.

Corresponding Author: Matthew L. Freedman, Medical Oncology, Dana-Farber Cancer Institute, Boston, MA 02215. Phone: 617-582-8598; Fax: 617-632-2165; E-mail: mfreedman@partners.org

Clin Cancer Res 2022;28:928–38

doi: 10.1158/1078-0432.CCR-21-3762

Translational Relevance

Early detection of neuroendocrine prostate cancer (NEPC) is challenging in clinical practice but has important prognostic and therapeutic implications for men with metastatic castration-resistant prostate cancer (mCRPC). In the largest study to date of cell-free DNA (cfDNA) from men with NEPC, we developed and validated a noninvasive NEPC Risk Score using tissue-informed cfDNA methylation analysis. Applying the NEPC Risk Score to cfDNA from two independent cohorts of men with mCRPC resulted in highly accurate discrimination between men with versus without NEPC. In both cohorts, high NEPC Risk Score was associated with significantly worse overall survival. These data strongly support the clinical utility of this cfDNA methylation–based NEPC Risk Score in men with mCRPC to noninvasively identify those who should be considered for platinum-based chemotherapy or clinical trials of novel NEPC-directed therapies.

cfDNA from men with NEPC or CR-PRAD. Finally, in an independent cfDNA cohort from men with NEPC or CR-PRAD, we confirm the analytical and clinical validity of this approach for accurate, noninvasive detection of NEPC.

Materials and Methods

Subjects and samples

Plasma samples were collected from men with mCRPC diagnosed and treated at the Dana-Farber Cancer Institute (DFCI), Brigham and Women's Hospital, or Weill Cornell Medicine (WCM) between April 2003 and August 2021. Two genitourinary pathologists (H.K. Tsai and M.S. Hirsch) confirmed the presence of high-grade neuroendocrine carcinoma of prostate origin according to modern conventions based on histologic review of available material, reinterpretation of original reports, and integration of available molecular results (10). Patients with CR-PRAD had castration-resistant prostate adenocarcinoma with no pathologic evidence of neuroendocrine differentiation throughout their disease course. All patients provided written informed consent. The use of samples was approved by the DFCI (01-045 and 09-171) and WCM (1305013903). Studies were conducted in accordance with recognized ethical guidelines. The previously described LuCaP patient-derived xenografts (PDX) were derived from resected metastatic prostate cancer with informed consent of patient donors under a protocol approved by the Institutional Review Board of University of Washington Human Subjects Division (11).

Sample processing

cfDNA samples were processed by the following method. Peripheral blood was collected in EDTA Vacutainer tubes (BD) and processed within 3 hours of collection. Plasma was separated by centrifugation at 2,500 × *g* for 10 minutes, transferred to microcentrifuge tubes, and centrifuged at 2,500 × *g* at room temperature for 10 minutes to remove cellular debris. The supernatant was aliquoted into 1 to 2 mL aliquots and stored at −80°C until the time of DNA extraction. cfDNA was isolated from 1 mL of plasma, using the QIAGEN Circulating Nucleic Acids Kit (QIAGEN), eluted in AE buffer, and stored at −80°C. DNA from the LuCaP PDXs was extracted using the DNeasy Blood and Tissue Kit (QIAGEN). Genomic DNA was sheared using a Covaris Sonicator E220, and AMPure XP beads (Beckman Coulter) were used to size select 150 to 250 bp DNA fragments.

cfDNA tumor content calculation

Low-pass whole-genome sequencing (LPWGS) was performed on all cfDNA samples. The ichorCNA R package was used to infer copy-number profiles and cfDNA tumor content from read abundance across bins spanning the genome using default parameters (12).

cfMeDIP-seq protocol

cfMeDIP-seq was performed using previously published methods (9). cfDNA library preparation was performed using the KAPA HyperPrep Kit (KAPA Biosystems) according to the manufacturer's protocol. We then performed end-repair, A-tailing, and ligation of NEBNext adaptors (NEBNext Multiplex Oligos for Illumina kit, New England BioLabs). Libraries were digested using the USER enzyme (New England BioLabs). λ DNA, consisting of unmethylated and *in vitro* methylated DNA, was added to prepared libraries to achieve a total amount of 100 ng DNA. Methylated and unmethylated *Arabidopsis thaliana* DNA (Diagenode) was added for quality control. MeDIP was performed using the MagMeDIP Kit (Diagenode) following the manufacturer's protocol. Samples were purified using the iPure Kit v2 (Diagenode). Success of the immunoprecipitation was confirmed using qPCR to detect recovery of the spiked-in *Arabidopsis thaliana* methylated and unmethylated DNA.

Next-generation sequencing (NGS) library construction

KAPA HiFi Hotstart ReadyMix (KAPA Biosystems) and NEBNext Multiplex Oligos for Illumina (New England Biolabs) were added to a final concentration of 0.3 μmol/L, and libraries were amplified as follows: activation at 95°C for 3 minutes, amplification cycles of 98°C for 20 seconds, 65°C for 15 seconds, 72°C for 30 seconds, and a final extension of 72°C for 1 minute. Samples were pooled and sequenced (Novogene Corporation) on Illumina HiSeq 4000 to generate 150 bp paired-end reads.

Quality control and processing of sequencing reads

After sequencing, the quality and quantity of the raw reads were examined using FastQC version 0.11.5 (http://www.bioinformatics.babraham.ac.uk/projects/fastqc) and MultiQC version 1.7 (13). Raw reads were quality and adapter trimmed using Trim Galore! version 0.6.0 (http://www.bioinformatics.babraham.ac.uk/projects/trim_galore/) using default settings in paired-end mode. The trimmed reads then were aligned to hg19 using Bowtie2 version 2.3.5.1 in paired-end mode and all other settings default (14). The SAMtools version 1.10 software suite was used to convert SAM alignment files to BAM format, sort and index reads, and remove duplicates (15). The R package RSamtools version 2.2.1 was used to calculate the number of unique mapped reads. Saturation analyses to evaluate reproducibility of each library were carried out using the R Bioconductor package MEDIPS version 1.38.0 (16).

Tissue-informed approach to NEPC detection

To identify differentially methylated regions (DMR) between NEPC and PRAD tumors, we first binned the genome into 300 base-pair windows and tested each window for differential methylation between NEPC and PRAD samples using limma-voom (using R package limma version 3.42.0) on TMM-normalized counts (using R package edgeR version 3.28.0; refs. 17, 18). Only bins with a total count above a fixed threshold were tested for differential methylation, where the threshold was set at 20% of the total number of samples across both groups. We restricted our search to bins within annotated CpG islands and FANTOM5 enhancers and excluded regions of high signal or poor mappability (19, 20). We selected DMRs with read enrichment in

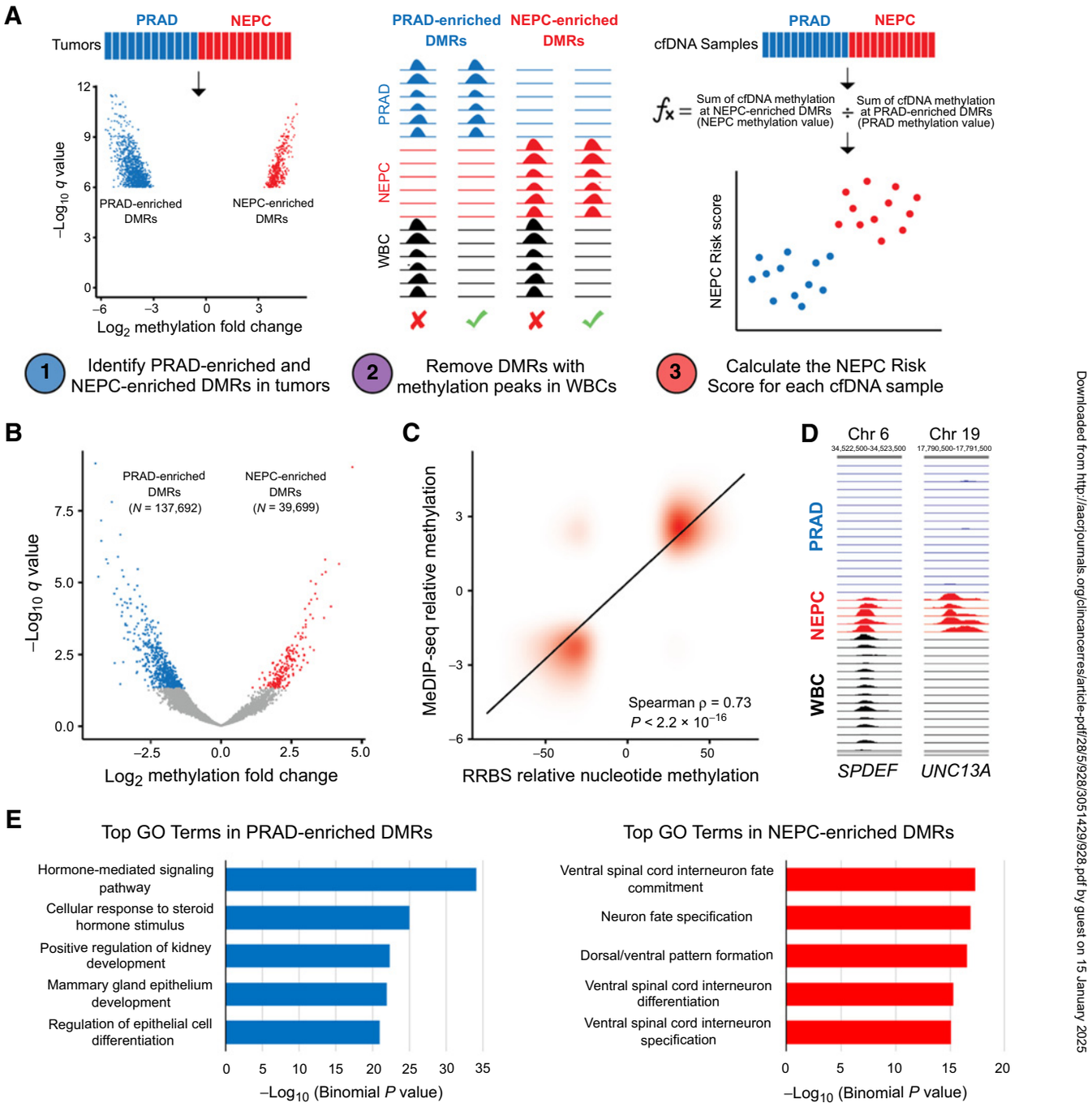

Figure 1.

Identification of tumor-derived PRAD-enriched and NEPC-enriched DMRs. **A,** Overview of the methods used to detect the presence of NEPC based on tissue-informed cfDNA analysis. **B,** Volcano plot showing DMRs between PRAD ($N = 24$) and NEPC ($N = 5$) PDXs. Red and blue dots represent PRAD-enriched ($N = 137,692$) and NEPC-enriched ($N = 39,699$) DMRs, respectively, with FDR-adjusted $P < 0.05$. **C,** Correlation between tumor-derived DMRs with differentially methylated nucleotides in reduced representation bisulfite sequencing (RRBS) data from CR-PRAD and NEPC tumors (4). **D,** Tracks depict methylation at the *SPDEF* gene and *UNC13A* gene determined by MeDIP-seq in PRAD tumors, NEPC tumors, and white blood cells (WBC). **E,** The top 5 gene ontology (GO) enrichment terms for PRAD-enriched and NEPC-enriched DMRs after removing sites with DNA methylation in WBCs.

NEPC compared with PRAD PDXs at FDR-adjusted $P < 1.0 \times 10^{-6}$ and $\log_2$ fold-change >3. We removed windows with peaks in MeDIP-seq data from white blood cells (as determined by MACS2, version 2.1.2) to minimize signal from blood cell–derived cfDNA (21). Using the MeDIPs R package, we calculated CpG-normalized relative methylation scores across 300 bp windows for each cfDNA sample (16, 22). We then summed relative methylation scores in cfDNA at NEPC-enriched PDX DMRs for each sample and normalized this value to the sum of rms values across all 300 bp windows. This value was termed "NEPC Methylation Value." The same process was performed for PRAD-enriched PDX DMRs to derive a "PRAD Methylation Value." We then calculated the $\log_2$ ratio of the NEPC Methylation Value to the PRAD Methylation Value and normalized these values to the median score in cfDNA from eight healthy cancer-free controls. This value was termed the "NEPC Risk Score." This approach is summarized in **Fig. 1A**.

Statistical analysis

Comparisons between two groups were calculated using a Wilcoxon rank-sum test. To determine the accuracy of the NEPC Risk Score for discriminating between cfDNA samples from men with NEPC versus CR-PRAD, the AUROC was calculated using JMP version 16. The optimal cutoff for classifying NEPC versus CR-PRAD samples based on NEPC Risk Scores in the cfDNA test cohort was calculated using Youden's index (J = sensitivity + specificity – 1). The optimal cutoff was determined as the point with the maximum index value. OS was defined as time from radiographic evidence of metastatic disease to death. Living patients were censored at the last evaluation. OS was estimated using the Kaplan–Meier method. P values were calculated using log-rank test. All P values were two-sided.

Data and materials availability

The cfMeDIP-seq NGS data for patient samples that support the findings of this study are available upon request from the corresponding author (M.L. Freedman) to comply with the DFCI ethics regulations to protect patient privacy. All requests for raw and analyzed data will be promptly reviewed by the Belfer Office for Dana-Farber Innovations to verify if the request is subject to any intellectual property or confidentiality obligations. Any data and materials that can be shared will be released via a Data Transfer Agreement. All codes used to process the data and carry out the analyses described in the methods are in a publicly available GitHub repository at https://github.com/scbaca/cfmedip.

Results

Identification of NEPC- and PRAD-enriched DMRs in a tumor training set

Prior applications of cfMeDIP-seq for noninvasive cancer detection identified DMRs directly in cfDNA between highly disparate patient groups, such as cancer versus no cancer (7–9). However, as men with mCRPC who develop NEPC often have concurrent PRAD, this limits the ability to identify NEPC-specific DMRs directly in cfDNA. To address this unique challenge, we developed a novel tissue–informed strategy for analyzing cfMeDIP-seq data (**Fig. 1A**). We first performed MeDIP-seq on 29 LuCaP PDXs, including 5 NEPC and 24 PRAD tumors (Supplementary Table S1; ref. 11). We chose to analyze PDXs based on recent single-cell analyses of mCRPC clinical biopsy specimens, which revealed significant intratumoral heterogeneity, including admixed NEPC and PRAD cell populations (23, 24). In contrast, the LuCaP PDXs, which have undergone comprehensive pathologic and molecular characterization, provide a more pure source of NEPC and PRAD tumor cells (11).

Differential methylation analysis of the LuCaP PDXs identified 39,699 NEPC-enriched and 137,692 PRAD-enriched DMRs (FDR-adjusted $P < 0.05$; **Fig. 1B**; ref. 11). To ensure that the PDX methylation data are representative of clinical biopsy specimens, we compared the LuCaP-derived NEPC- and PRAD-enriched DMRs with DNA methylation data generated from an independent set of castration-resistant NEPC and PRAD tumors using reduced-representation bisulfite sequencing (4). We observed a high correlation between NEPC- and PRAD-enriched DMRs from the LuCaP PDXs and the clinical biopsy specimens ($\rho = 0.73$; $P < 2.2 \times 10^{-16}$; **Fig. 1C**).

We then identified a subset of NEPC- and PRAD-enriched DMRs that could be used to noninvasively detect NEPC. Using a stringent cutoff of FDR-adjusted $P < 1.0 \times 10^{-6}$ and $\log_2$ fold-change >3, we identified 432 NEPC-enriched and 1,086 PRAD-enriched DMRs. As the majority of cfDNA is derived from leukocytes, we removed sites that were methylated in WBCs from age-matched male controls ($N =$ 1,165), resulting in a final set of 76 NEPC-enriched and 277 PRAD-enriched DMRs. The *SPDEF* gene highlights the importance of this step. Although *SPDEF* was methylated in NEPC and unmethylated in PRAD tumors, it is also methylated in WBCs (**Fig. 1D**). The inability to determine whether a methylated cfDNA fragment at this locus originated from NEPC or WBCs renders it uninformative for detecting NEPC and could contribute to misclassification. As exemplified in *UNC13A*, a gene associated with neural signaling, the final set of DMRs are methylated in one tumor type and unmethylated in the opposite

Table 1. Patient characteristics at the time of cfDNA collection in the test and validation cohorts of men with mCRPC.

	cfDNA Test cohort		cfDNA Validation cohort	
	NEPC ($N = 9$)	PRAD ($N = 39$)	NEPC ($N = 12$)	PRAD ($N = 41$)
Median cfDNA tumor content (range)	15% (5.1%–75%)	21% (3.3%–80%)	23% (3.4%–43%)	16% (3.8%–49%)
Median age (range)	72 (60–84)	71 (61–92)	71 (54–91)	70 (49–86)
Median PSA (range)	0.37 (0.03–3.7)	140 (0.79–4,305)	0.33 (0.01–6.23)	112 (4.5–1,821)
De novo NEPC	3 (33%)	N/A	2 (17%)	N/A
Prior local therapy	5 (56%)	27 (69%)	5 (42%)	26 (63%)
Prior ADT	4 (44%)	39 (100%)	8 (67%)	41 (100%)
Prior abiraterone or enzalutamide	0 (0%)	36 (92%)	4 (33%)	39 (95%)
Prior docetaxel	2 (22%)	25 (64%)	2 (17%)	35 (85%)
Prior EP chemotherapy	7 (78%)	0 (0%)	8 (67%)	0 (0%)
Liver metastases	3 (33%)	15 (38%)	8 (67%)	13 (32%)

Abbreviations: EP, etoposide plus platinum; N/A, not applicable.

tumor type and WBCs. Consequently, cfDNA fragments at these loci indicate the presence of NEPC or PRAD.

To ensure that the final set of tumor-derived DMRs retained biological relevance, we assessed nearby genes for GO term enrichment (25). The top GO terms in NEPC-enriched DMRs pertained to neural development and differentiation, whereas PRAD-enriched DMRs related to hormone signaling and epithelial cell differentiation, suggesting that the final set of tumor-derived DMRs reflect the divergent gene regulatory programs of NEPC and PRAD (**Fig. 1E**).

Classification of NEPC and CR-PRAD samples in a cfDNA test cohort

To evaluate the ability to accurately detect NEPC using the novel tissue–informed approach, we analyzed a test cohort of plasma cfDNA samples from 56 men with mCRPC, including 11 with NEPC and 45 with CR-PRAD. We first performed LPWGS on all cfDNA samples and calculated tumor content using ichorCNA, an analytical tool that estimates cfDNA tumor fraction based on somatic copy-number alterations (12). Based on the ichorCNA lower limit of detection (3% tumor fraction), 48 (86%) of the 57 cfDNA samples had detectable tumor DNA including 9 (82%) and 39 (87%) of patients with NEPC and CR-PRAD, respectively (12). cfDNA samples with less than 3% tumor content were excluded from methylation analysis (Supplementary Fig. S1). These results compare favorably to a published cfDNA analysis of 269 samples from men with metastatic prostate cancer that detected tumor DNA in 83% of samples using LPWGS and hybrid-capture targeted sequencing (26).

Characteristics of men in the cfDNA test cohort at the time of plasma collection are listed in **Table 1**. Consistent with known decoupling of prostate-specific antigen (PSA) from its typical association with disease burden in NEPC, the median PSA was 0.37 for patients with NEPC (range, 0.03–3.7) and 140 for patients with CR-PRAD (range, 0.79–4,305; ref. 10). Median cfDNA tumor content was 15% for men with NEPC (range, 5.1%–75%) and 21% for those with CR-PRAD (range, 3.3%–80%; $P = 0.89$; **Table 1**; Supplementary Fig. S2A).

To evaluate the ability to detect NEPC in cfDNA from men with mCRPC, we first performed cfMeDIP-seq on the test cohort samples. We then derived an NEPC Methylation Value and PRAD Methylation Value for each sample by summing the methylated cfDNA fragments at tissue-derived NEPC-enriched and PRAD-enriched DMRs, respectively (**Fig. 1A**). An NEPC Risk Score was calculated for each sample as the normalized ratio of the NEPC Methylation Value versus the PRAD Methylation Value.

We observed significantly higher NEPC Methylation Values in men with NEPC than CR-PRAD (median 8.1×10^{-6} vs. 6.3×10^{-6}; $P = 0.0025$; **Fig. 2A**). In contrast, PRAD Methylation Values were significantly higher in men with CR-PRAD than NEPC (median 5.4×10^{-5} vs. 4.1×10^{-5}; $P = 4.3 \times 10^{-6}$; **Fig. 2B**). NEPC Risk Scores were significantly higher in men with NEPC than those with CR-PRAD (median 0.35 vs. −0.14; $P = 4.3 \times 10^{-7}$; **Fig. 2C**). The AUROC for accurate classification of men with NEPC versus CR-PRAD based on NEPC Risk Score was 0.96. The optimal NEPC Risk Score cutoff (high >0.15 vs. low ≤0.15) demonstrated 100% sensitivity and 90% specificity for detecting NEPC. Further, high versus low NEPC Risk Score was associated with significantly shorter OS from the time of metastatic prostate cancer [HR = 2.5; 95% confidence interval (95% CI), 1.2–4.8; $P = 0.017$; **Fig. 2D**]. Median OS was 32 months shorter for men with high (14 months) versus low (46 months) NEPC Risk Scores.

Classification of NEPC and CR-PRAD samples in an independent cfDNA validation cohort

To assess the reproducibility of this approach and the NEPC Risk Score cutoff, we identified an independent multi-institutional validation cohort of plasma samples from 73 men with mCRPC at DFCI and WCM, including 16 men with NEPC and 57 with CR-PRAD. cfDNA LPWGS identified tumor DNA in 53 (73%) samples including 12 (75%) and 48 (72%) patients with NEPC and CR-PRAD, respectively. cfDNA samples with less than 3% tumor content were excluded from methylation analysis (Supplementary Fig. S1). Median cfDNA tumor content was 23% for patients with NEPC (range, 3.4%–43%) and 16% for patients with CR-PRAD (range, 3.8%–39%) in the test cohort ($P = 0.49$; Supplementary Fig. S2B; **Table 1**). Median PSA was 0.33 (range, 0.01–6.23) in men with NEPC versus 112 (range, 4.5–1,821) in those with CR-PRAD. Differences between men with NEPC and CR-PRAD

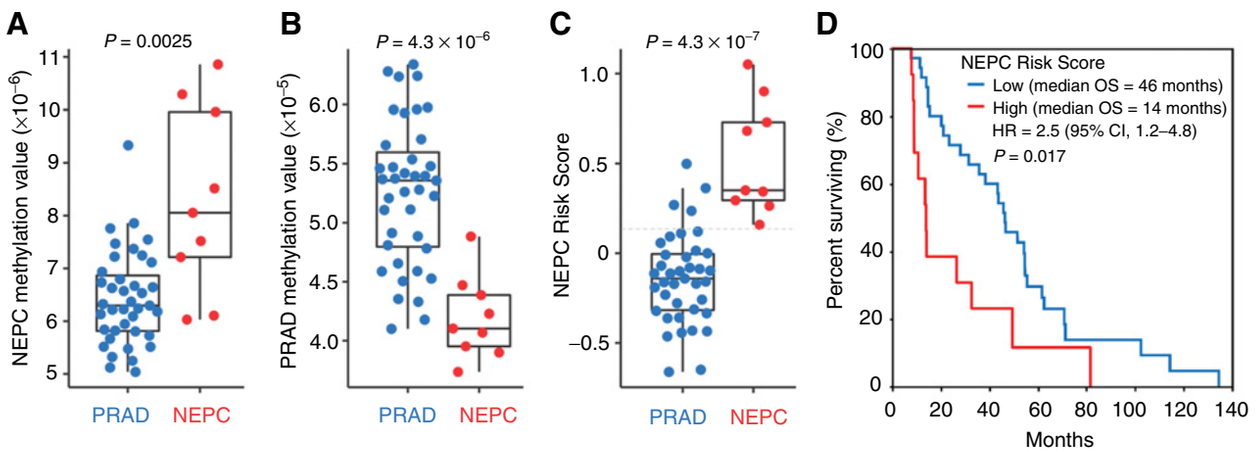

Figure 2.

Classification of NEPC and PRAD samples in the cfDNA test cohort. NEPC Methylation Values (**A**), PRAD Methylation Values (**B**), and NEPC Risk Scores (**C**) in cfDNA samples from men with PRAD or NEPC in the test cohort. *P* values calculated using a two-sided Wilcoxon rank-sum test. Optimal cutoff (indicated by dotted gray line) was determined in this cohort using Youden's J statistic. **D,** Kaplan–Meier curve for OS from the time of metastatic disease for men with high (>0.15) versus low (≤0.15) NEPC Risk Score relative to the cutoff.

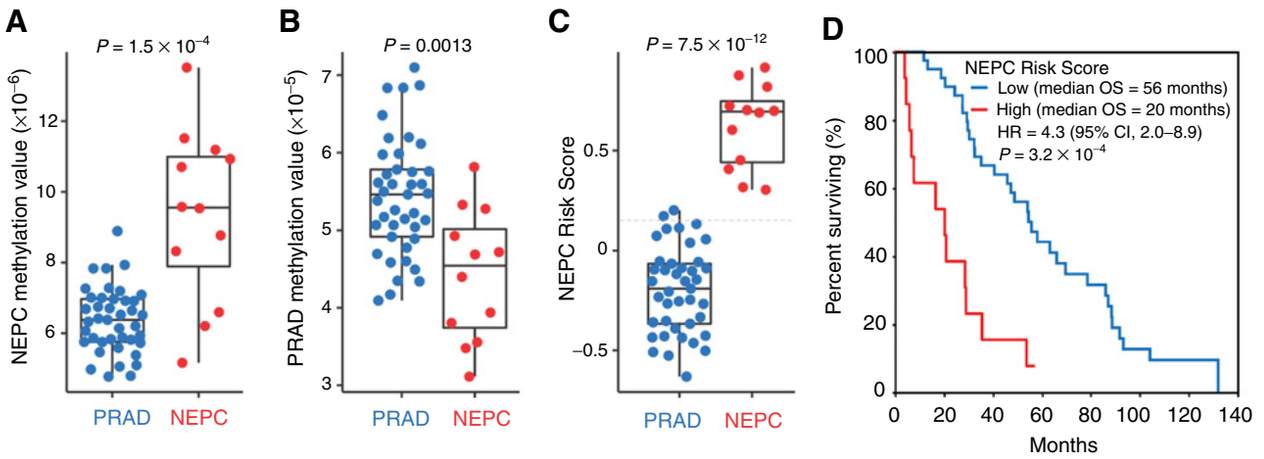

Figure 3.

Classification of NEPC and PRAD samples in the cfDNA validation cohort. NEPC Methylation Values (**A**), PRAD Methylation Values (**B**), and NEPC Risk Scores (**C**) in cfDNA samples from men with NEPC or PRAD in the validation cohort. *P* values calculated using a two-sided Wilcoxon rank-sum test. The optimal NEPC Risk Score cutoff determined in the independent cfDNA test cohort is indicated by dotted gray line. **D,** Kaplan–Meier curve for OS from the time of metastatic disease for men with high (>0.15) versus low (≤0.15) NEPC Risk Score relative to the cutoff determined in the independent cfDNA test cohort.

in the cfDNA validation cohort were similar to those observed in the cfDNA test cohort (**Table 1**).

As we observed in the test cohort, NEPC samples in the cfDNA validation cohort exhibited significantly higher NEPC Methylation Values (median 9.6×10^{-6} vs. 6.4×10^{-6}; $P = 1.5 \times 10^{-4}$), lower PRAD Methylation Values (median 4.5×10^{-5} versus 5.5×10^{-5}; $P = 0.0013$), and higher NEPC Risk Scores (median 0.69 vs. −0.19; $P = 7.5 \times 10^{-12}$) than those with CR-PRAD (**Fig. 3A–C**). The AUROC for accurate classification of men with NEPC versus CR-PRAD based on NEPC Risk Score was 1.0. Applying the NEPC Risk Score cutoff derived in the test cohort (high >0.15 vs. low ≤0.15) to the cfDNA validation cohort resulted in 100% sensitivity and 95% specificity for detecting NEPC. High versus low NEPC Risk Score was associated with significantly shorter OS from the time of metastatic prostate cancer (HR = 4.3; 95% CI, 2.9–8.9; $P = 3.2 \times 10^{-4}$; **Fig. 3D**). Median OS was 36 months shorter for men with high (20 months) versus low (56 months) NEPC Risk Scores. Notably, there was no association of cfDNA tumor content with OS across the two cfDNA cohorts (Supplementary Fig. S3), suggesting that the negative correlation between NEPC Risk Score and OS is driven by different tumor biology and not higher disease burden.

Patient vignettes highlight NEPC risk factors in misclassified CR-PRAD samples

To understand potential factors driving misclassification, we reviewed medical histories for the six patients with CR-PRAD with NEPC Risk Scores >0.15 across the two cfDNA cohorts. Five of these patients had clinical, radiographic, and genomic features associated with NEPC (**Fig. 4**). The two patients with the highest NEPC Risk Score (0.50 and 0.36) both previously received abiraterone, docetaxel, and cabazitaxel and were on enzalutamide at the time of cfDNA collection. The first patient's CT scan 6 days after cfDNA collection showed marked increase in metastatic tumor burden, including new liver metastases. He subsequently experienced clinical deterioration

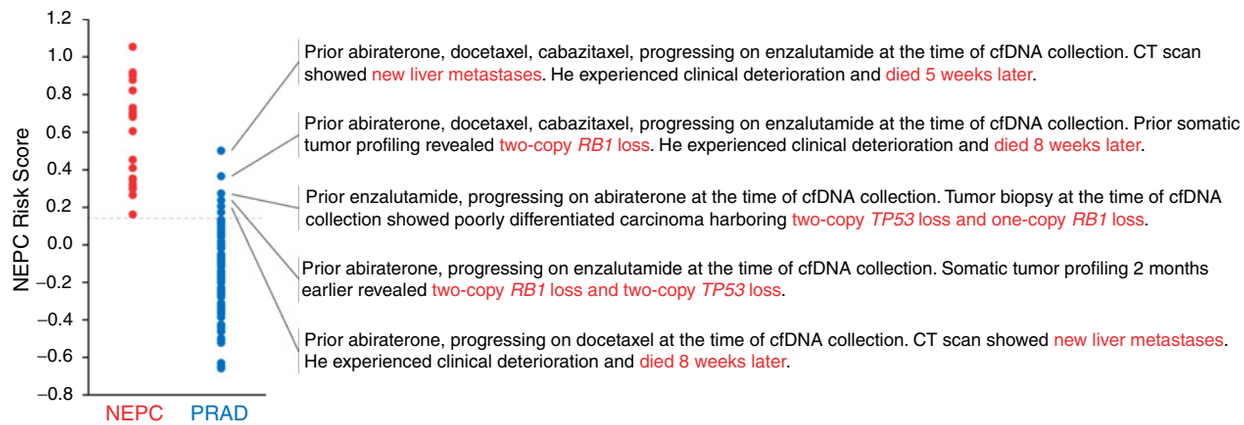

Figure 4.

cfDNA from men with CR-PRAD with high NEPC Risk Scores displays clinical and genomic features of NEPC.

and died 5 weeks later. The second patient previously underwent somatic tumor profiling revealing two-copy *RB1* deletion. He experienced clinical deterioration and died 8 weeks after cfDNA collection. The next three patients had all received prior abiraterone and/or enzalutamide. The first (NEPC Risk Score of 0.27) was progressing on abiraterone and underwent tumor biopsy at the time of cfDNA collection showing poorly differentiated carcinoma harboring single-copy *RB1* loss and two deleterious *TP53* alterations. The second patient (NEPC Risk Score of 0.24) previously received abiraterone and was progressing on enzalutamide at the time of cfDNA collection. Genomic profiling 2 months earlier showed that the patient's tumor harbored biallelic loss of *RB1* and *TP53*. The third patient (NEPC Risk Score of 0.20) previously received abiraterone and at the time of cfDNA collection was progressing on docetaxel with CT scan showing new liver metastases. He experienced clinical deterioration and died 2 months later. These hypothesis-generating vignettes suggest the possibility that the cfDNA NEPC Risk Score may identify occult NEPC not detected through routine clinical care.

Association of the plasma cfDNA methylome with NEPC risk score and tumor content

Prior data suggest that the plasma cfDNA methylome strongly correlates with tumor content in men with metastatic prostate cancer (27). As such, we sought to understand the association of the cfDNA methylome in this cohort with tumor content. We first performed principal component analysis (PCA) of the genome-wide methylome data (**Fig. 5A**) and the methylation data at the NEPC- and PRAD-enriched DMRs included in the NEPC Risk Score (**Fig. 5B**) for the 101 cfDNA samples included in the NEPC Risk Score analyses. In the genome-wide data, the first principal component (PC1) was driven by an outlier sample with high CpG enrichment relative to the others. There was otherwise no separation of NEPC and CR-PRAD samples in PC1 and PC2 in the genome-wide methylome data (**Fig. 5A**). However, at the DMR sites, PC1 and PC2 clearly separated NEPC and CR-PRAD samples (**Fig. 5B**).

We next quantified the correlation between each of the first 10 PCs with NEPC Risk Score and cfDNA tumor content. For the genome-wide data, not until PC8, which explained 2.2% of variance, was there a robust correlation with NEPC Risk Score ($R^2 = 0.32$; $P = 7.3 \times 10^{-10}$; **Fig. 5C**; Supplementary Fig. S4A). In contrast, when limiting to the DMRs included in the NEPC Risk Score, PC1 ($R^2 = 0.34$; $P = 1.2 \times 10^{-10}$), which explained 30% of variance, and PC2 ($R^2 = 0.42$; $P = 2.0 \times 10^{-13}$), which explained 8.3% of variance, both demonstrated robust correlation with NEPC Risk Score (**Fig. 5D**; Supplementary Fig. S4B). We then quantified the correlation between the top PCs and cfDNA tumor content. In the genome-wide methylome data, PC2, which explained 4.2% of variance, correlated with cfDNA tumor content ($R^2 = 0.34$; $P = 1.7 \times 10^{-10}$; **Fig. 5E**; Supplementary Fig. S4A). This result affirms the prior finding that the prostate cancer plasma cfDNA methylome correlates with cfDNA tumor content (27). When limiting to the DMRs included in the NEPC Risk Score, PC1 ($R^2 = 0.22$; $P = 7.2 \times 10^{-7}$) and PC2 ($R^2 = 0.29$; $P = 5.1 \times 10^{-9}$) correlated with cfDNA tumor content, though not to the same extent they correlated with NEPC Risk Score (**Fig. 5F**; Supplementary Fig. S4B).

Finally, we assessed the correlation between NEPC Risk Score and cfDNA tumor content (**Fig. 5G**). Across all NEPC and CR-PRAD cfDNA samples, there was no correlation between NEPC Risk Score and tumor content ($R^2 = 0.0033$; $P = 0.57$); there was also no correlation in the PRAD samples ($R^2 = 0.010$; $P = 0.37$). NEPC Risk Score and tumor content did significantly correlate in the cfDNA samples from men with NEPC ($R^2 = 0.24$; $P = 0.025$). Given this association, suggesting lower NEPC Risk Scores in men with lower cfDNA tumor content, we evaluated the diagnostic performance of the NEPC Risk Score in the NEPC and CR-PRAD samples across the two cohorts with cfDNA tumor content less than 10%. The NEPC Risk Score in these patients resulted in an AUROC of 0.93; applying the NEPC Risk Score cutoff of 0.15 resulted in 100% sensitivity and 82% specificity for detecting NEPC (data not shown).

Discussion

NEPC is an aggressive, clinically actionable resistance phenotype that can emerge in men with mCRPC. The challenge of identifying NEPC in routine clinical practice leads to delays in diagnosis and underdiagnosis. In the largest study to date of cfDNA from men with NEPC, we present a novel approach for tissue-informed analysis of cfMeDIP-seq data, leading to highly accurate noninvasive detection of NEPC. We first identified methylation sites enriched in a training set of NEPC and PRAD tumors. Tissue-informed methylation analysis of two independent cohorts of cfDNA from men with pathologically confirmed NEPC or CR-PRAD demonstrated high accuracy (AUROC of 0.96 and 1.0). Importantly, applying a diagnostic cutoff derived in the cfDNA test cohort to the independent validation cohort resulted in 100% sensitivity and 95% specificity for detecting NEPC. Finally, in both cfDNA cohorts, a high NEPC Risk Score was associated with significantly shorter OS (HR of 2.5 and 4.3). This work strongly supports the analytical and clinical utility of tissue-informed analysis of cfMeDIP-seq data to noninvasively detect NEPC in men with mCRPC.

The current approach for diagnosing NEPC has significant shortcomings that could be overcome with a liquid biopsy. The lack of consensus pathologic criteria highlights the advantage of an objective biomarker. Herein, we demonstrated that tissue-informed analysis of cfMeDIP-seq data provide a quantitative readout (NEPC Risk Score) that discriminated between men with NEPC or CR-PRAD with high accuracy in two independent cfDNA cohorts. The ability to apply a diagnostic cutoff from one cfDNA cohort to an independent cohort while maintaining excellent diagnostic accuracy suggests this quantitative approach is robust and reproducible. An additional benefit of a liquid biopsy to detect NEPC is that cfDNA may be more representative of a patient's overall tumor burden than tissue biopsy of a single metastatic focus (28). Intrapatient tumor heterogeneity is well established in mCRPC (5). This is highly relevant in this clinical context, as NEPC often emerges as a treatment-resistant subclone and can be missed due to sampling error with a single tissue biopsy. Future studies analyzing cfDNA from patients undergoing autopsy or correlating cfDNA results with molecular imaging could provide further insight into how representative NEPC Risk Scores are of intrapatient NEPC versus PRAD tumor burden. However, we establish is this report that the NEPC Risk Score is a highly accurate quantitative noninvasive biomarker that is highly predictive of the presence or absence of NEPC in men with mCRPC.

Detecting NEPC has important prognostic implications. Compared with men with CR-PRAD, NEPC is associated with shorter OS (1). Consistent with this known negative prognostic association, we observed that high NEPC Risk Score (relative to the diagnostic cutoff) was associated with significantly shorter OS in two independent cfDNA cohorts. Aggarwal and colleagues reported an HR of 1.8 (95% CI, 1.0–3.2) for OS in men with versus without treatment-emergent small-cell NEPC (1). The HRs for OS in our cohorts were 2.5 (95% CI, 1.2–4.8) and 4.3 (95% CI, 2.0–8.9). The worse prognosis

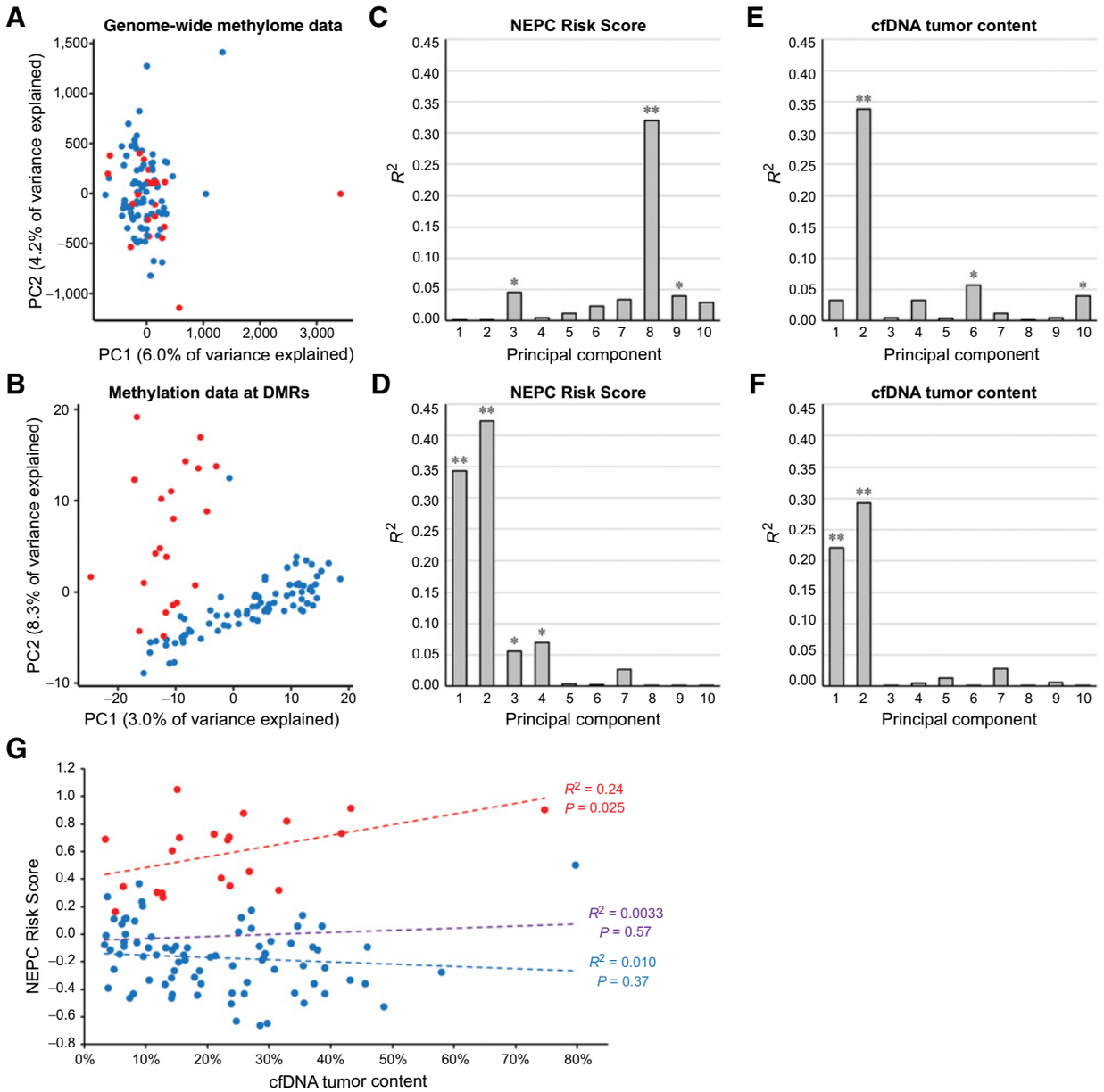

Figure 5.

Association of the plasma cfDNA methylome with NEPC Risk Score and tumor content. **A,** PCA of the genome-wide methylome for 101 plasma cfDNA samples from men with CR-PRAD or NEPC. **B,** PCA of the 101 plasma cfDNA samples limiting to the NEPC- and PRAD-enriched DMRs included in the NEPC Risk Score. Correlation between NEPC Risk Score with the top 10 PCs for the cfDNA genome-wide methylome data (**C**) and restricted to the DMR sites (**D**). Correlation between cfDNA tumor content with the top 10 PCs for the cfDNA genome-wide methylome data (**E**) and restricted to the DMR sites (**F**). Correlation between NEPC Risk Score and each PC was measured using the coefficient of determination (R^2). *, $P < 0.05$; **, $P < 1 \times 10^{-6}$. **G,** Correlation between NEPC Risk Score and tumor content for the 101 cfDNA samples from men with NEPC and CR-PRAD. Dotted lines show the linear regression for the NEPC samples (red), CR-PRAD samples (blue), and all samples (purple).

of men with high NEPC Risk Score in our study may reflect differences in patient characteristics. We included only men with morphologic high-grade neuroendocrine carcinoma and not PRAD with expression of neuroendocrine markers by immunohistochemistry—the latter is not as clearly associated with a virulent clinical course as the former (10).

Early and accurate detection of NEPC also has important therapeutic implications. Although men with NEPC are characteristically unresponsive to ARSIs, they are more likely to respond to platinum-based chemotherapy (3). Consequently, NCCN guidelines recommend treatment with platinum chemotherapy combined with etoposide or a taxane (29). Histology-specific treatment recommendations

highlight the immediate clinical actionability of detecting NEPC. With several ongoing clinical trials testing novel therapeutic approaches in men with NEPC, the implications of detecting this disease variant will likely increase in the coming years (30). Although the association of the NEPC Risk Score with response to prostate cancer therapy remains to be established, we encourage incorporating cfDNA collection into prospective clinical trials to facilitate future studies to develop and validate noninvasive biomarkers to identify patients likely to benefit from NEPC-directed therapy.

Successful cfDNA-based biomarkers must be accurate, cost-effective, and practical to implement in clinical practice. Beltran and colleagues previously reported the feasibility of noninvasively detecting NEPC-specific DNA methylation in cfDNA using whole-genome bisulfite sequencing (WGBS; ref. 6). However, test characteristics for distinguishing men with NEPC versus CR-PRAD using this approach were not reported. Compared with WGBS, cfMeDIP-seq has several advantages. The high cost of whole-genome sequencing currently limits the ability to implement WGBS in clinical practice. In contrast, by only sequencing methylated cfDNA, cfMeDIP-seq provides genome-wide methylation data at a fraction of the cost of WGBS. Further, cfMeDIP-seq only requires 5 to 10 ng of cfDNA, which can be obtained from 1 mL of plasma. Although direct comparison of the performance of these approaches will be informative, the low cost, small sample requirement, and high sensitivity highlight advantages of cfMeDIP-seq as the basis for a clinical biomarker.

The methods presented in this article represent an important advance for developing cfDNA methylation–based clinical biomarkers. Several recent publications highlight advantages of epigenetic compared with genetic liquid biopsy approaches (31–33). Whereas previous studies performed unsupervised analysis of cfMeDIP-seq data, we developed a novel tissue–informed method, which benefits from the strength of its biological basis. Tissue-informed analysis ensures that the model is built upon molecular features known to be present in and specific to the tumor of interest. This contrasts with the tumor-naïve approach of developing a methylation signature directly in cfDNA (e.g., from individuals with cancer vs. without cancer), which risks overfitting due to signal unrelated to cancer (e.g., sex, age, smoking status, comorbid disease, etc.). PCA emphasized the value of this tissue-informed approach. In the genome-wide cfDNA methylome data, not until PC8, which explained only 2.2% of variance, did we observe a correlation with the methylation signal that distinguished NEPC from CR-PRAD samples. However, the methylation data at the tissue-derived NEPC- and PRAD-enriched DMRs revealed a strong correlation between NEPC Risk Score and PCs 1 and 2, which explained nearly 40% of variance. We believe that the methods presented herein will help facilitate detection of clinically relevant cancer phenotypes. Aberrant DNA methylation is present across tumor types with several clinically actionable subtypes harboring distinct methylation profiles, such as *IDH*-mutant gliomas and microsatellite instability–high uterine and colon cancers (34–37). As our understanding of clinically actionable epigenetically-distinct cancer phenotypes evolves, the methods presented in this article will facilitate noninvasive detection of these tumor subtypes.

Although our results strongly support the feasibility of using cfMeDIP-seq to noninvasively detect NEPC in men with mCRPC, it is appropriate to recognize several potential limitations. First, is the number of patients with NEPC included in the study? The cfDNA test and validation cohorts contained 21 men with NEPC. Although this number is small in absolute terms, it represents the largest analysis to date of cfDNA from men with pathologically confirmed NEPC. Although similarly high accuracy was observed across two independent cfDNA cohorts, the reproducibility and clinical validity will benefit from further prospective validation. It is also important to acknowledge that this was a retrospective and heterogeneous cohort, which introduces potential confounding factors, mainly patient selection. This limits our ability to conclusively establish that NEPC Risk Score is associated with inferior clinical outcomes. However, that the NEPC Risk Score performs so well despite the heterogeneity in the cohort speaks to the robustness of the methylation signal and the ability of the assay and methods to detect it. Another limitation is that patients with NEPC in this study were limited to men with high-grade neuroendocrine carcinoma and did not include those with PRAD with neuroendocrine differentiation (10). Thus, we cannot comment on whether the NEPC Risk Score discriminates between these two variants. Likewise, all men in the NEPC group had biopsy-proven high-grade neuroendocrine carcinoma at the time of plasma collection. We did not evaluate plasma samples in men prior to NEPC diagnosis when the relative abundance of NEPC-derived cfDNA may be lower and thus harder to detect. As such, we were not able to establish how early in the disease course this biomarker can detect treatment-emergent NEPC. Finally, as we limited the methylation analysis to men with detectable circulating tumor DNA by ichorCNA, we did not assess how the assay performs in men with very low cfDNA tumor content. More work is needed to fully establish the relationship between NEPC Risk Score with cfDNA tumor content. Several additional questions remain: What is the analytical limit of detection of this cfDNA methylation–based approach for detecting NEPC? What is the optimal timing to evaluate cfDNA in men with mCRPC to identify NEPC? How long before clinical diagnosis can NEPC be detected in cfDNA? Will early detection and initiation of platinum-based chemotherapy improve clinical outcomes for men diagnosed with NEPC? We hope to address these questions in future studies.

In summary, we demonstrated the analytical and clinical utility of tissue-informed cfDNA methylation analysis to noninvasively detect NEPC in men with mCRPC. These findings support further studies to establish the prognostic and predictive value of the cfDNA NEPC Risk Score in men with mCRPC. Finally, the novel methods reported in this article are an important step toward broadening the clinical applicability of blood-based epigenomic assays by providing a framework for noninvasive detection of tumor subtypes with distinct DNA methylation profiles.

Authors' Disclosures

J.E. Berchuck reports personal fees from UroToday, personal fees and other support from Genome Medical, and other support from Cityblock Health outside the submitted work; in addition, J.E. Berchuck has a patent for Methods for identifying NEPC with tissue-informed cfDNA methylation analysis pending. S.C. Baca reports personal fees from Nuscan Diagnostics outside the submitted work; in addition, S.C. Baca has a patent for methods for identifying NEPC pending and owns equity in Nuscan Diagnostics. V. Conteduca reports speaker honoraria or travel support from Astellas, Janssen-Cilag, and Sanofi-Aventis; consulting fees from Bayer; and an advisory board position at Janssen, AstraZeneca, and Merck. O. Elemento reports other support from Freenome during the conduct of the study; O. Elemento also reports grants, personal fees, and other support from Volastra Therapeutics, as well as other support from OneThree Biotech outside the submitted work. E. Corey reports other support from AbbVie, Janssen Research, Forma Therapeutics, Arvinas, GSK, Bayer, Kronos, and Foghorn during the conduct of the study. M.-E. Taplin reports personal fees from Janssen, AstraZeneca, Roviant, Epizyme, Constellation, Myovant, Bayer, AbbVie, Astellas, and Arcus Bioscience outside the submitted work. T.K. Choueiri reports personal fees from Foundation Medicine, non-financial support and other support from Guardant, and grants from DOD grant during the conduct of the study. T.K. Choueiri also reports grants, personal fees, and non-financial support from Pfizer, Exelixis, BMS, Merck, Roche/Genentech, Eisai, Lilly, and EMD; personal fees from Up-to-Date; and other support from Nuscan Diagnostics, Tempest, Pionyr, and Osel outside the submitted work. T.K. Choueiri received travel and accommodation

support (pre-COVID) in relation to consulting, advisory roles, or honoraria when travel needed; is a member of prior ASCO/ESMO educational and scientific committees (GU Cancers); and has a medical writing support in relation to articles. Finally, T.K. Choueiri has a patent for ctDNA pending and is listed as an inventor on patents filed that pertain to the data presented in this manuscript. H. Beltran reports grants and other support from Janssen; other support from AstraZeneca, Merck, Foundation Medicine, Pfizer, Blue Earth Diagnostics, Amgen, and Oncorus; and grants from Bristol Myers Squibb outside the submitted work. M.L. Freedman reports other support from Nuscan Diagnostics outside the submitted work; in addition, M.L. Freedman has a patent for detecting NEPC using DNA methylation pending. No disclosures were reported by the other authors.

Authors' Contributions

J.E. Berchuck: Conceptualization, data curation, formal analysis, supervision, funding acquisition, validation, investigation, visualization, methodology, writing–original draft, project administration, writing–review and editing. **S.C. Baca:** Conceptualization, software, formal analysis, validation, investigation, visualization, methodology, writing–review and editing. **H.M. McClure:** Investigation, writing–review and editing. **K. Korthauer:** Software, methodology. **H.K. Tsai:** Data curation, investigation, methodology. **P. Vitale Nuzzo:** Methodology. **K.M. Kelleher:** Data curation. **M. He:** Data curation. **J.A. Steinharter:** Data curation. **S. Zacharia:** Formal analysis. **S. Spisak:** Methodology. **J.-H. Seo:** Supervision, investigation, methodology. **V. Conteduca:** Data curation. **O. Elemento:** Data curation. **J. Auh:** Data curation. **M. Sigouros:** Resources, data curation. **E. Corey:** Resources, data curation, supervision. **M.S. Hirsch:** Resources, data curation, supervision. **M.-E. Taplin:** Conceptualization, supervision, funding acquisition, writing–review and editing. **T.K. Choueiri:** Resources, data curation, supervision. **M.M. Pomerantz:** Conceptualization, resources, data curation, supervision, funding acquisition, validation, writing–review and editing. **H. Beltran:** Conceptualization, resources, data curation, supervision, funding acquisition, validation, methodology, writing–review and editing. **M.L. Freedman:** Conceptualization, resources, data curation, supervision, funding acquisition, methodology, writing–review and editing.

Acknowledgments

J.E. Berchuck is supported by the Department of Defense (W81XWH-20-1-0118). S.C. Baca is supported by a fellowship from the PhRMA Foundation and the Kure It Cancer Research Foundation. K. Korthauer is supported by the Natural Sciences and Engineering Research Council of Canada. Establishment and characterization of the LuCaP PDX models have been supported by the Pacific Northwest Prostate Cancer SPORE (P50CA97186), the Department of Defense Prostate Cancer Biorepository Network (W81XWH-14-2-0183), the National Cancer Institute P01 CA163227, the Prostate Cancer Foundation, the Institute for Prostate Cancer Research, and the Richard M. Lucas Foundation. M.M. Pomerantz, H. Beltran, and M.L. Freedman are supported by a DFCI Medical Oncology grant award. H. Beltran is supported by the National Cancer Institute (5R37CA241486). M.L. Freedman is supported by the Claudia Adams Barr Program for Innovative Cancer Research, the H.L. Snyder Medical Research Foundation, and the Cutler Family Fund for Prevention and Early Detection.

The costs of publication of this article were defrayed in part by the payment of page charges. This article must therefore be hereby marked *advertisement* in accordance with 18 U.S.C. Section 1734 solely to indicate this fact.

Received October 19, 2021; revised November 12, 2021; accepted December 10, 2021; published first December 13, 2021.

References

1. Aggarwal R, Huang J, Alumkal JJ, Zhang L, Feng FY, Thomas GV, et al. Clinical and genomic characterization of treatment-emergent small-cell neuroendocrine prostate cancer: A multi-institutional prospective study. J Clin Oncol 2018;36:2492–503.
2. Abida W, Cyrta J, Heller G, Prandi D, Armenia J, Coleman I, et al. Genomic correlates of clinical outcome in advanced prostate cancer. Proc Natl Acad Sci U S A 2019;116:11428–36.
3. Humeniuk MS, Gupta RT, Healy P, McNamara M, Ramalingam S, Harrison M, et al. Platinum sensitivity in metastatic prostate cancer: Does histology matter? Prostate Cancer Prostatic Dis 2018;21:92–9.
4. Beltran H, Prandi D, Mosquera JM, Benelli M, Puca L, Cyrta J, et al. Divergent clonal evolution of castration-resistant neuroendocrine prostate cancer. Nat Med 2016;22:298–305.
5. Gundem G, Van Loo P, Kremeyer B, Alexandrov LB, Tubio JMC, Papaemmanuil E, et al. The evolutionary history of lethal metastatic prostate cancer. Nature 2015;520:353–7.
6. Beltran H, Romanel A, Conteduca V, Casiraghi N, Sigouros M, Franceschini GM, et al. Circulating tumor DNA profile recognizes transformation to castration-resistant neuroendocrine prostate cancer. J Clin Invest 2020;130:1653–68.
7. Shen SY, Singhania R, Fehringer G, Chakravarthy A, Roehrl MHA, Chadwick D, et al. Sensitive tumour detection and classification using plasma cell-free DNA methylomes. Nature 2018;563:579–83.
8. Shen SY, Burgener JM, Bratman SV, De Carvalho DD. Preparation of cfMeDIP-seq libraries for methylome profiling of plasma cell-free DNA. Nat Protoc 2019;14:2749–80.
9. Nuzzo PV, Berchuck JE, Korthauer K, Spisak S, Nassar AH, Abou Alaiwi S, et al. Detection of renal cell carcinoma using plasma and urine cell-free DNA methylomes. Nat Med 2020;26:1041–3.
10. Epstein JI, Amin MB, Beltran H, Lotan TL, Mosquera J-M, Reuter VE, et al. Proposed morphologic classification of prostate cancer with neuroendocrine differentiation. Am J Surg Pathol 2014;38:756–67.
11. Nguyen HM, Vessella RL, Morrissey C, Brown LG, Coleman IM, Higano CS, et al. LuCaP prostate cancer patient-derived xenografts reflect the molecular heterogeneity of advanced disease and serve as models for evaluating cancer therapeutics. Prostate 2017;77:654–71.
12. Adalsteinsson VA, Ha G, Freeman SS, Choudhury AD, Stover DG, Parsons HA, et al. Scalable whole-exome sequencing of cell-free DNA reveals high concordance with metastatic tumors. Nat Commun 2017;8:1324.
13. Ewels P, Magnusson M, Lundin S, Käller M. MultiQC: Summarize analysis results for multiple tools and samples in a single report. Bioinforma Oxf Engl 2016;32:3047–8.
14. Langmead B, Salzberg SL. Fast gapped-read alignment with Bowtie 2. Nat Methods 2012;9:357–9.
15. Li H, Handsaker B, Wysoker A, Fennell T, Ruan J, Homer N, et al. The sequence alignment/map format and SAMtools. Bioinforma Oxf Engl 2009;25:2078–9.
16. Lienhard M, Grimm C, Morkel M, Herwig R, Chavez L. MEDIPS: Genome-wide differential coverage analysis of sequencing data derived from DNA enrichment experiments. Bioinforma Oxf Engl 2014;30:284–6.
17. Law CW, Chen Y, Shi W, Smyth GK. voom: Precision weights unlock linear model analysis tools for RNA-seq read counts. Genome Biol 2014;15:R29.
18. Robinson MD, Oshlack A. A scaling normalization method for differential expression analysis of RNA-seq data. Genome Biol 2010;11:R25.
19. Cavalcante RG, Sartor MA. annotatr: Genomic regions in context. Bioinformatics 2017;33:2381–3.
20. Amemiya HM, Kundaje A, Boyle AP. The ENCODE blacklist: Identification of problematic regions of the genome. Sci Rep 2019;9:9354.
21. Zhang Y, Liu T, Meyer CA, Eeckhoute J, Johnson DS, Bernstein BE, et al. Model-based analysis of ChIP-Seq (MACS). Genome Biol 2008;9:R137.
22. Pelizzola M, Koga Y, Urban AE, Krauthammer M, Weissman S, Halaban R, et al. MEDME: An experimental and analytical methodology for the estimation of DNA methylation levels based on microarray derived MeDIP-enrichment. Genome Res 2008;18:1652–9.
23. Cejas P, Xie Y, Font-Tello A, Lim K, Syamala S, Qiu X, et al. Subtype heterogeneity and epigenetic convergence in neuroendocrine prostate cancer. Nat Commun 2021;12:5775.
24. Dong B, Miao J, Wang Y, Luo W, Ji Z, Lai H, et al. Single-cell analysis supports a luminal-neuroendocrine transdifferentiation in human prostate cancer. Commun Biol 2020;3:778.

25. McLean CY, Bristor D, Hiller M, Clarke SL, Schaar BT, Lowe CB, et al. GREAT improves functional interpretation of cis-regulatory regions. Nat Biotechnol 2010;28:495–501.
26. Mayrhofer M, De Laere B, Whitington T, Van Oyen P, Ghysel C, Ampe J, et al. Cell-free DNA profiling of metastatic prostate cancer reveals microsatellite instability, structural rearrangements and clonal hematopoiesis. Genome Med 2018;10:85.
27. Wu A, Cremaschi P, Wetterskog D, Conteduca V, Franceschini GM, Kleftogiannis D, et al. Genome-wide plasma DNA methylation features of metastatic prostate cancer. J Clin Invest 2020;130:1991–2000.
28. Wyatt AW, Annala M, Aggarwal R, Beja K, Feng F, Youngren J, et al. Concordance of circulating tumor DNA and matched metastatic tissue biopsy in prostate cancer. J Natl Cancer Inst 2017;109:djx118.
29. National Comprehensive Cancer Network. NCCN clinical practice guidelines in oncology: prostate cancer (Version 1.2022) [Internet]. 2021. Available from: https://www.nccn.org/professionals/physician_gls/pdf/prostate.pdf.
30. Berchuck JE, Viscuse PV, Beltran H, Aparicio A. Clinical considerations for the management of androgen indifferent prostate cancer. Prostate Cancer Prostatic Dis 2021;24:623–37.
31. Lasseter K, Nassar AH, Hamieh L, Berchuck JE, Nuzzo PV, Korthauer K, et al. Plasma cell-free DNA variant analysis compared with methylated DNA analysis in renal cell carcinoma. Genet Med 2020;22:1366–73.
32. Parikh AR, Seventer EEV, Siravegna G, Hartwig AV, Jaimovich A, He Y, et al. Minimal residual disease detection using a plasma-only circulating tumor DNA assay in colorectal cancer patients. Clin Cancer Res 2021;27:5586–94.
33. Liu MC, Oxnard GR, Klein EA, Swanton C, Seiden MV, Liu MC, et al. Sensitive and specific multi-cancer detection and localization using methylation signatures in cell-free DNA. Ann Oncol 2020;31:745–59.
34. Saghafinia S, Mina M, Riggi N, Hanahan D, Ciriello G. Pan-cancer landscape of aberrant DNA methylation across human tumors. Cell Rep 2018;25:1066–80.
35. Noushmehr H, Weisenberger DJ, Diefes K, Phillips HS, Pujara K, Berman BP, et al. Identification of a CpG island methylator phenotype that defines a distinct subgroup of glioma. Cancer Cell 2010;17:510–22.
36. CGA Network. Comprehensive molecular characterization of human colon and rectal cancer. Nature 2012;487:330–7.
37. CGAR Network, Kandoth C, Schultz N, Cherniack AD, Akbani R, Liu Y, et al. Integrated genomic characterization of endometrial carcinoma. Nature 2013;497:67–73.